General Disclaimer

One or more of the Following Statements may affect this Document

- This document has been reproduced from the best copy furnished by the organizational source. It is being released in the interest of making available as much information as possible.

- This document may contain data, which exceeds the sheet parameters. It was furnished in this condition by the organizational source and is the best copy available.

- This document may contain tone-on-tone or color graphs, charts and/or pictures, which have been reproduced in black and white.

- This document is paginated as submitted by the original source.

- Portions of this document are not fully legible due to the historical nature of some of the material. However, it is the best reproduction available from the original submission.

Produced by the NASA Center for Aerospace Information (CASI)

NASA Contractor Report 156845

Oceanic Geoid and Tides Obtained from GEOS-3 Satellite Data in the Northwestern Atlantic Ocean

(NASA-CR-156845) OCEANIC GEOID AND TIDES OBTAINED FROM GEOS-3 SATELLITE DATA IN THE NORTHWESTERN ATLANTIC OCEAN (North Carolina State Univ.) 26 p HC A03/MF A01 CSCL 08C

N79-12679

Unclas

G3/48 38020

I.J. Won and L.S. Miller

October 1978

DEC 1978
RECEIVED
NASA STI FACILITY

NASA
National Aeronautics and
Space Administration

Wallops Flight Center
Wallops Island, Virginia 23337
AC 804 824-3411

TABLE OF CONTENTS

Introduction	1
Analysis of Linear Satellite Data for Oceanic Geoid and Tides	3
Results of Analysis of Simulated Data	6
Description of the GEOS-3 Data Used for the Analysis	8
Results of GEOS-3 Data Analysis	13
Conclusions	19
Acknowledgements	20
References	21

LIST OF FIGURES

Figure		Page
1	Locations of the two strips of data in the GEOS-3 calibration area used for the analysis.	4
2	Results of simulated study.	7
3	Profiles for the 28 south-going paths between Newfoundland and Cuba.	9
4	Profiles for the 26 north-going paths between Puerto Rico and the North Carolina coast.	10
5	South-going amplitude and phase profiles for M_2, O_1, S_2 and K_1 tides obtained from altimeter data using 5th, 6th and 8th order Tchevichev polynomial representations.	15
6	North-going amplitude and phase profiles for M_2, O_1, S_2 and K_1 tides.	16

LIST OF TABLES

Table		
1	Characteristics of GEOS-3 Data Used for Analysis and the Locations of Reference Paths	12
2	RMS Error Amplitudes (cm) of the Residual Altimeter Data after Removing Geoid and Tides for 40 Different Analyses	17

Introduction

A precise geopotential model has become increasingly important as more satellites, particularly those designed for geodetic and altimetry purposes, require accurate orbital tracking to produce meaningful results from their orbital data. The geoid model, the static part of the geopotential field, has been rapidly improved using various data from satellite tracking and surface gravity in terms of the order and degree of spherical harmonic expansion. Most recent models may include NASA's Goddard Space Flight Center geoid based on the work of Marsh and Vincent (1974), GEM 9 and 10 by Lerch et al (1977), and one reported by Gaposchkin and Mendes (1977), the last two models having the degree and order 30.

Most importantly, the geoid model cannot be significantly improved until we know the distribution of the open ocean tides. Since tides are regarded as noise in deriving a geoid model, the RMS error amplitude of the resultant geoid can not be theoretically smaller than the RMS amplitude of tides. Those geoid models having residual amplitudes less than a few meters may have already reached this barrier. To break this barrier, we are inevitably led to consider a technique which is capable of simultaneously deriving both geoid and tides from satellite altimeter data.

Satellite altimeter data consist of ocean elevation measurements with respect to a reference spheroid along subsatellite tracks distributed more or less randomly both in space and time. The mapping of the tides using these data is considerably more difficult both mathematically and computationally than that required for a static geoid and requires a far greater amount of altimeter data with higher accuracy. This is not only because of the dynamic nature of the tides, but also their relatively small amplitudes, generally less than one meter worldwide.

Zetler and Maul (1971) performed a study using simulated satellite altimeter data on the tidal analysis at a fixed location. They assumed that the tidal height at a given time would be uniform over a 5° square area and that they

could use the altimeter data whenever the satellite passed over the area. A randomly sampled time series thus generated may be solved for tides by the least-squares harmonic method. They showed that it was possible to retrieve major tidal constituents from the simulated data in the presence of random noise which was larger than the signal.

Maul and Yanaway (1977) applied this method to GEOS-3 data obtained within a 5° x 5° square centered at 30°N and 70°W (near Bermuda Island). They regarded the data falling in this square as a time-series of a single location and applied a least-square harmonic analysis method which is regularly used for conventional tidal analysis. The results they obtained showed that the tidal amplitudes from the GEOS-3 data were an order of magnitude higher than those obtained from the MODE deep-sea tide gauge, and their solution did not converge when the size of the square was changed. Therefore, they concluded that it was not possible to retrieve tides from GEOS-3 data.

Won et al (1977) developed a similar least-square harmonic analysis method which is designed to simultaneously extract both the oceanic geoid and tides for a surface (rather than for a single point) using satellite altimeter data. In their case, both the geoid and tides within a region are represented by a set of two-dimensional functions. By applying this method to sets of simulated data in the northeastern Pacific Ocean, they showed that tides whose amplitude may be as small as 10 cm may be retrieved from the simulated data even when the data are contaminated with ±1 meter random noise.

Both studies described above assume that the error in the altimeter data is random and has no orbital drift. However, the most severe difficulty in using altimeter data for the tidal analysis stems from orbital bias error. Marsh et al (1976) investigated the problem with the Skylab altimeter data, and found the error is position-dependent and is of long wavelength nature (~100°) with amplitudes on the order of several meters. The orbital bias error of GEOS-3 has been steadily improved since its launch and stabilized

to less than a meter in the Calibration Area (H. R. Stanley, personal communication, 1977).

Determination of ocean tides for the entire northern Atlantic may require several hundred paths for a duration of a year or more, based on the simulated study by Won et al (1977). Since available data on hand are limited, we present in this paper the results of the oceanic geoid and four major tides, M_2, O_1, S_2, and K_1, obtained along two linear paths of GEOS-3 as shown in Figure 1. We shall briefly discuss the analytic method, results of a simulated study to test the method, and finally the results of actual GEOS-3 data.

Analysis of Linear Satellite Data for Oceanic Geoid and Tides

The conventional tidal analysis technique requires a long time series obtained at a fixed point to obtain its tidal spectrum. Since the altimeter data are obtained more or less randomly in time and space, this method is not applicable. The following method follows closely that by Won et al (1977) originally developed for a two dimensional tidal analysis.

Let us consider $H(x,t)$ the ocean height with respect to a reference spheroid at a distance x away from an arbitrary origin along the ground path of a satellite. Neglecting transient sea surface changes, we write

$$H(x,t) = C_o(x) + \sum_i A_i(x) \cos\{\omega_i t + \kappa_i(x)\} \tag{1}$$

where $C_o(x)$: constant ocean height, i.e., ocean geoid.

$A_i(x)$, $\kappa_i(x)$: amplitude and phase of i-th tidal component,

ω_i: frequency of i-th tidal imponent, and

t: time after the start of measurement

Since $\kappa_i(x)$ is continuous only in the interval of 0 to 2π, we use instead

$$\begin{Bmatrix} C_i(x) \\ S_i(x) \end{Bmatrix} = A_i(x) \begin{Bmatrix} \cos \kappa_i(x) \\ \sin \kappa_i(x) \end{Bmatrix} \tag{2}$$

ORIGINAL PAGE IS
OF POOR QUALITY

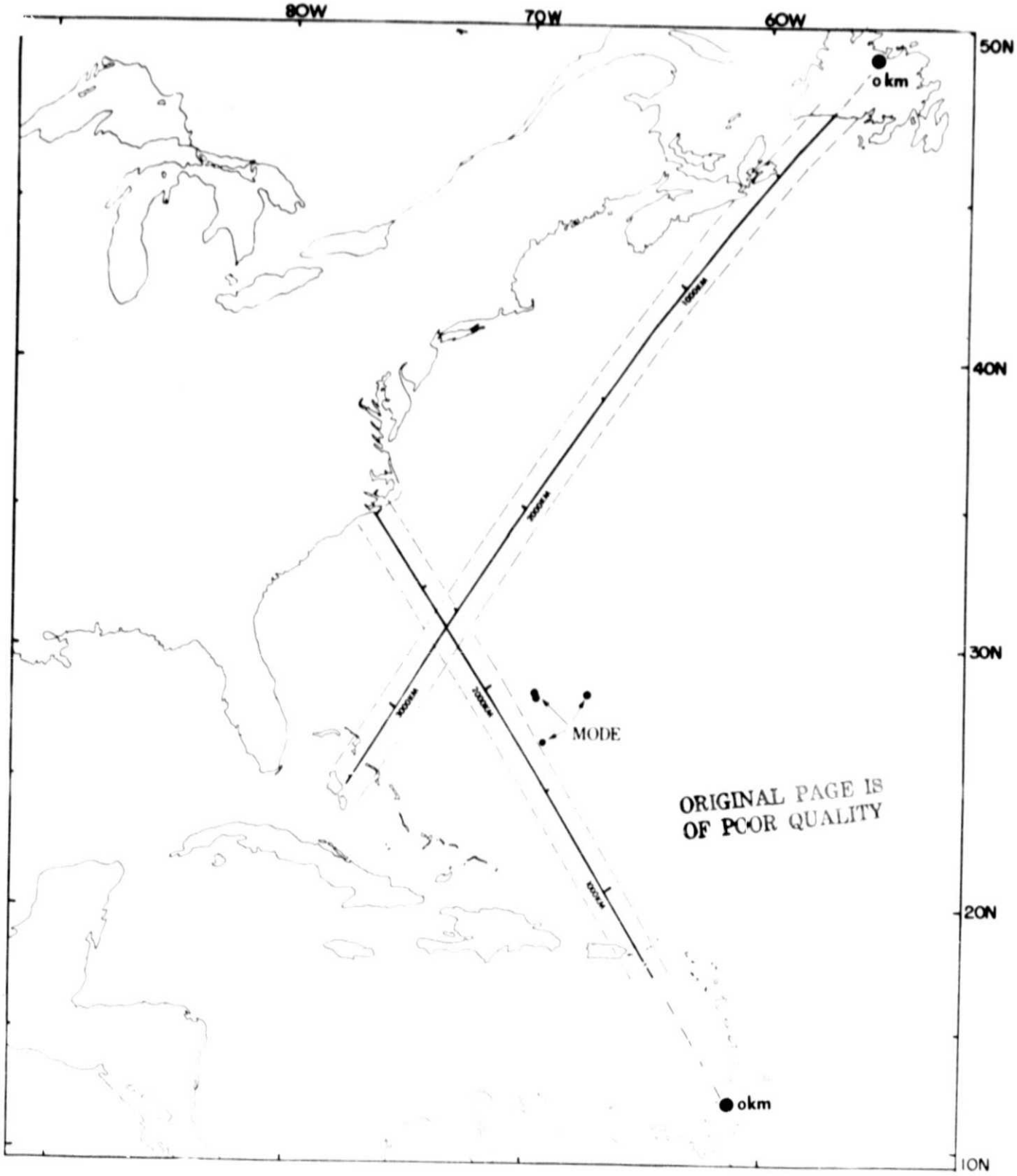

ORIGINAL PAGE IS
OF POOR QUALITY

Figure 1. Locations of the two strips of data in the GEOS-3 calibration area used for the analysis. The origin for counting linear distance is shown as a solid circle for each strip. The width of the strips is approximately 265 Km at 30°N latitude.

and let C_i and S_i, respectively, be represented by a polynomial series such that

$$\begin{Bmatrix} C_i(x) \\ S_i(x) \end{Bmatrix} = \sum_k \begin{Bmatrix} c_k^i \\ s_k^i \end{Bmatrix} T_k(x) \tag{3}$$

where $T_k(x)$ is any elementary function of order k in x.

For a given set of N altimeter data $F(x_j, t_j)$; $j = 1, 2 \ldots\ldots N$, we wish to find the best fitting $H(x,t)$ so that the quantity

$$S = \sum_{j=1}^{N} [F(x_j, t_j) - H(x_j, t_j)]^2 \tag{4}$$

be minimized with respect to c_k^i and s_k^i.

When the geoid and tides, respectively, are approximated by N_g and N_t order functions and L independent tidal components are sought, the equation (4) generates a positive-definite symmetric matrix of order $N_g + 2N_tL$.

There are two serious sources of measurement error (Brown et al 1976) which can completely invalidate the scheme presented here. The first source is, of course, the random measurement error of instrument. However, as shown by Zetler and Maul (1971), Won et al (1977), Maul (1977), and in this report, this error can be overcome as long as it is random.

The second error source, much more serious and seemingly unresolvable, is that caused by the uncertainty of satellite orbit, frequently referred to as orbital bias error. For example, the results reduced from the GEOS-3 altimeter data in the Calibration Area show that the sea surface heights along a given ground path, when compared with a model geoid, deviate as much as 20 meters. In addition, linear drift is typically about 3 meters per 1000 km along a ground path. The errors are mainly attributed to uncertainties in geopotential models used for satellite tracking.

The critical problem in tidal analysis is that these orbital bias errors will be aliased into any tidal spectrum. The problem can be more serious if the orbital period of a satellite is in resonance with any tidal period. One

possible method is incorporating the orbital bias error into equation (4) by assuming that the bias is represented by a polynomial for each path. In other words, instead of (4), we minimize

$$S' = \sum_p \sum_j [F(x_j,t_j) - \{H_p(x_j,t_j) + \sum_m a_m^p x_j^m\}]^2 \qquad (5)$$

where the subscript p denotes quantities in the p-th path only.

Results of Analysis of Simulated Data

To construct a realistic ocean surface as a function of space and time, we used a satellite geoid to the degree and order 20 by Rapp (1974) and amplitude and phase maps of M_2 and O_1 tides by Tiron et al (1967) in the northeastern Pacific Ocean. We arbitrarily chose one path similar to that of GEOS-3 and reconstructed the sea surface height data along this path. The geoid undulation along this path amounts to about 30 m, while the tides are less than 1m everywhere. For the given GEOS-3 orbital period (102 minutes) and inclination (65°), the data are collected whenever the mathematical satellite passes over within 2° in longitude on either side of the equator crossing of the designated path. Sampling time was chosen to $\approx$ 3.2 seconds, (approximately 22 km in distance) similar to that of GEOS-3. One data set thus generated is comprised of 2000 altimeter data points from 16 paths, each path about 3000 km long, covering 29.2 days.

A random series having a two meter peak-to-peak amplitude range is then generated in order to artificially contaminate the simulated data. The white noise series has a mean of near zero and an RMS amplitude of 58.4 cm. The series is then piecewise added to each path on a point-by-point basis.

When the noise was not added to the data, the reproduced geoid and tidal profiles were almost identical to the prescribed ones as shown in solid lines in Figure 2. The figure also shows results when the data were dubbed with 1 meter (dashed lines) and 2 meter (broken lines) noise.

ORIGINAL PAGE IS
OF POOR QUALITY

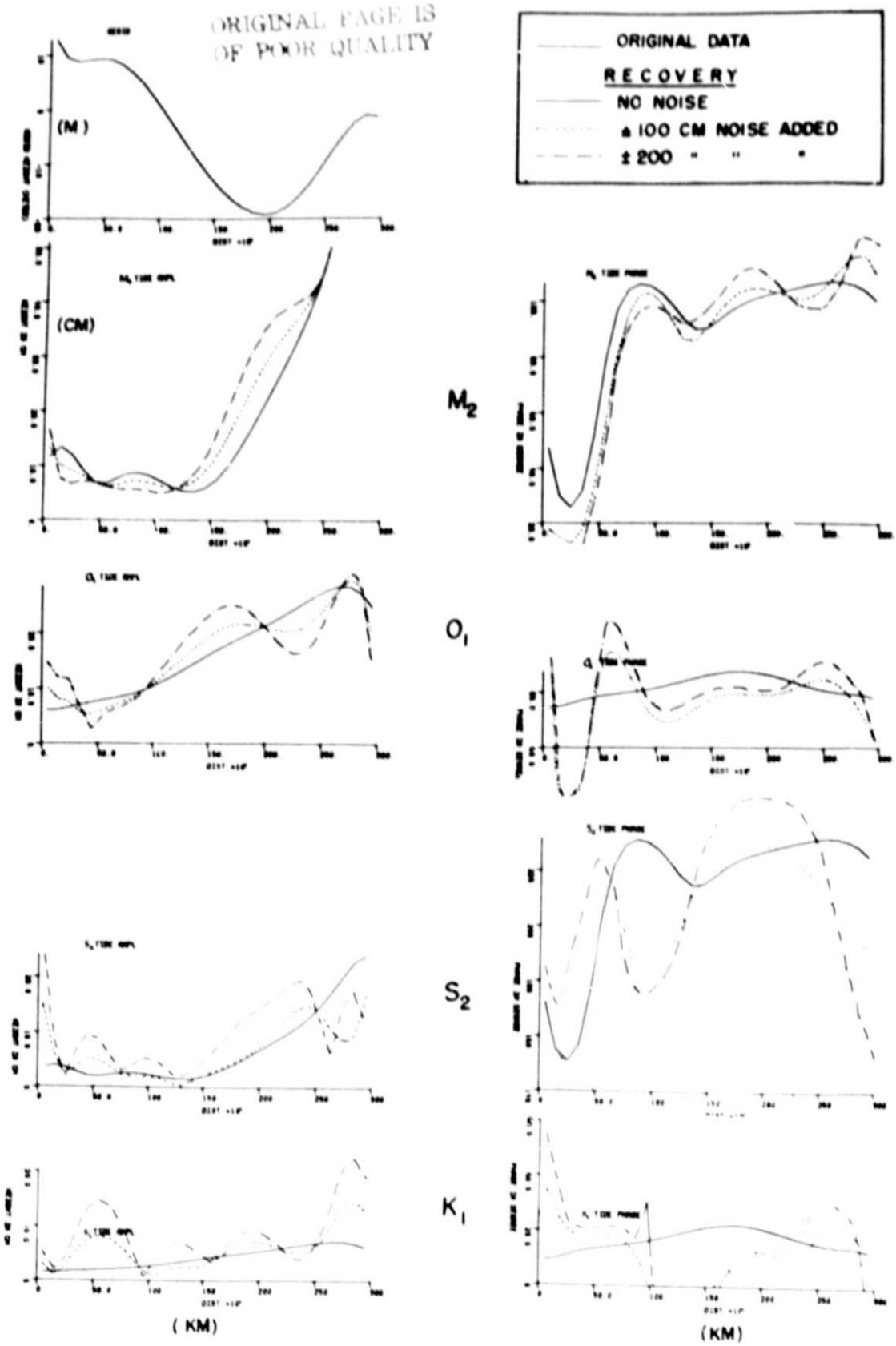

Figure 2. Results of simulated study. Solid lines show the original profiles of a geoid and four tides used for computing 2000 ocean height data. When no noise is added to the data, the results are indistinguishable. Recovered geoids coincide for all cases.

In all cases, the reproduction of the geoid is assured. While tidal signals are mostly well below the RMS noise amplitude, their recovery is reasonably good. Several factors contribute to the successful recovery: (1) the added noise is Gaussian, (2) no artificial drift within each path (such as the orbital bias error) is allowed, and (3) tidal frequencies are precisely known.

Description of the GEOS-3 Data Used for the Analysis

Two sets of GEOS-3 altimeter data confined in two narrow strips (Figure 1) are chosen for present analysis. One strip, starting at Newfoundland and ending at Cuba, consists of 28 south-going paths whose equator crossings are between 99.64°E and 102.46°E. The width of the strip is about 284 km at the equator and narrows somewhat toward higher latitude. The other strip, starting from near Puerto Rico and ending at the North Carolina coast, consists of 26 north-going paths whose equator crossings are between 53.54°W and 56.36°W. The data duration for both paths is about 17 months, starting April, 1975, and represent about 70% of the total available data within these two strips during that period.

The first two graphs of Figures 3 and 4 show the original altimeter sea-surface height data along with geoid heights computed from the Goddard Space Flight Center Marsh-Vincent geopotential model. It is evident that the orbital bias error is large, compared with the computed geoidal height frequently exceeding 10 m or more.

The initial data preparation for each strip proceeds as follows:

Step 1. Select a hypothetical reference path through the middle of the strip and project each data point onto the reference path along a line on which the distance between the data point and the reference path is minimum.

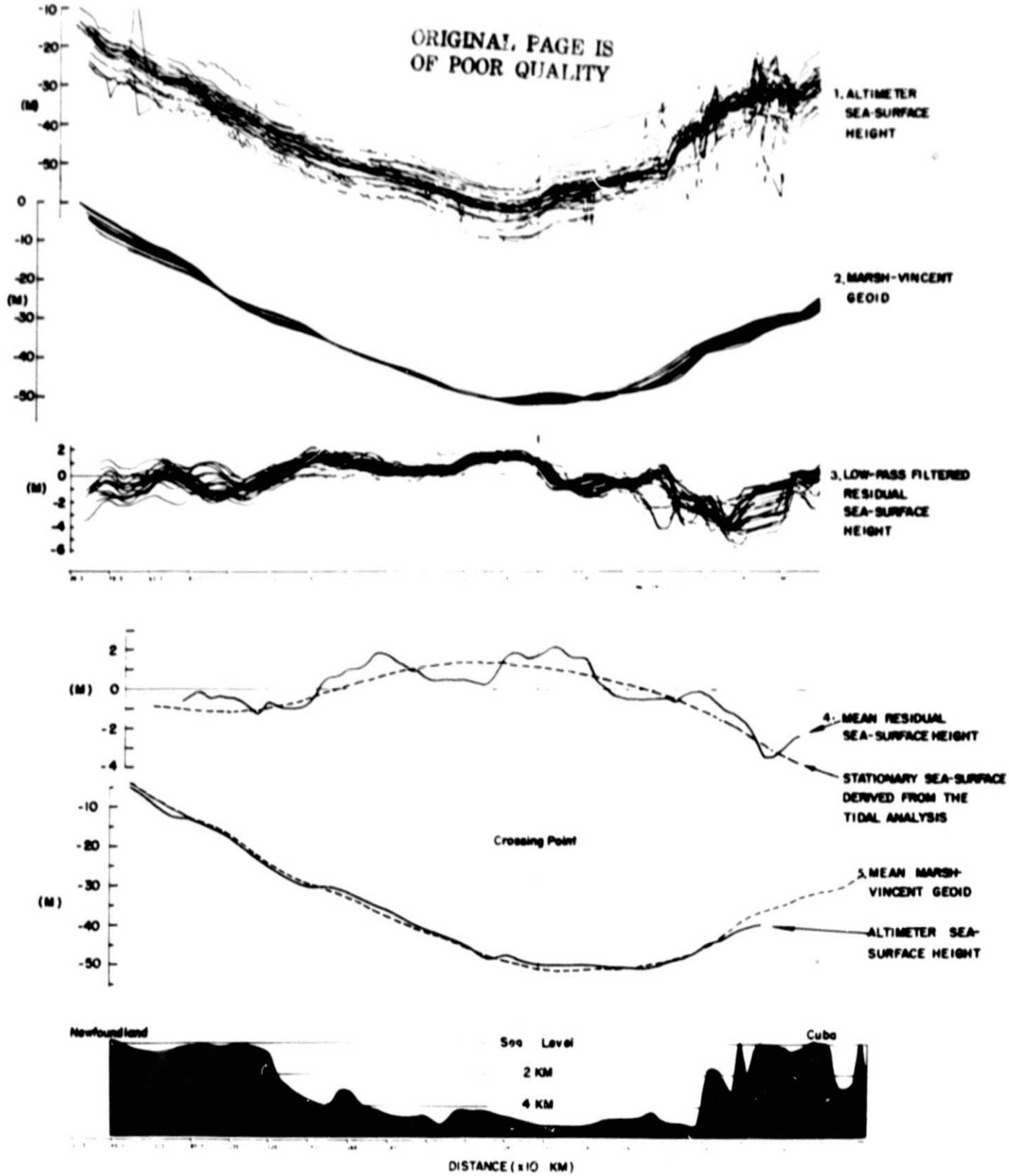

Figure 3. Profiles for the 28 south-going paths between Newfoundland and Cuba showing (1) Original data, (2) Computed geoid, (3) Residual sea-surface height, (4) Comparison between the mean residual sea-surface height and the residual geoid computed from the tidal analysis, (5) Comparison between the mean computed geoid and that added with the residual geoid.

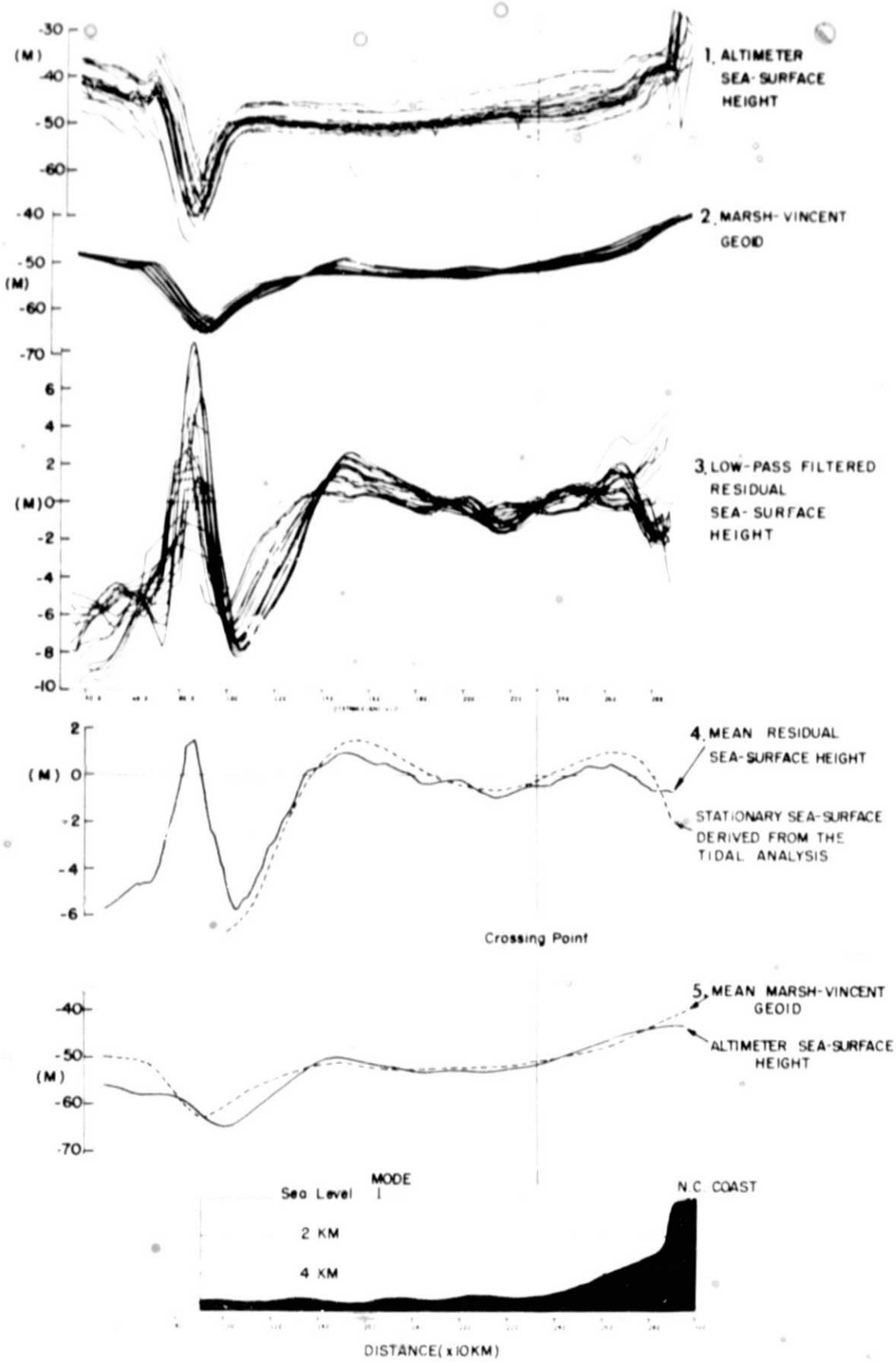

Figure 4. Profiles for the 26 north-going paths between Puerto Rico and the North Carolina coast. Refer to Figure 3 for explanation.

Step 2. Assign an arbitrary origin on the reference path and compute the great circle distance for each data point with respect to this origin. This step assimilates the original altimeter data into a single set of linear data as a function of distance.

Step 3. Remove bad data points.

Step 4. For data which fall in a specified interval distance, compute and remove a best-fitting linear function for each path. The results are shown in the third graphs of Figures 3 and 4.

It should be pointed out that during the last step any geoidal or tidal fluctuation whose wavelengths are longer than the spatial length is irretrievably lost. Furthermore, any nonlinear orbit drift is not removed and will affect the subsequent analysis. While any geoidal fluctuation whose wavelength is greater than about 1200 km is supposedly included in the Marsh-Vincent geoid, similar argument may not hold for the tidal fluctuation.

The characteristics of the GEOS-3 data used for this analysis are summarized in Table 1. The locations of the reference paths are also shown in Table 1 as well as in Figure 1. The final data set resulting from this preliminary preparation is then used for the least-square space-time harmonic analysis as described in the previous section in order to simultaneously obtain the tides and the residual ocean geoid.

TABLE 1. Characteristics of GEOS-3 Data Used for Analysis and the Locations of Reference Paths

	SOUTH-GOING STRIP	NORTH-GOING STRIP
a. Number of paths used	28	26
b. Duration	May 1975-Aug 1976	Apr 1975-Aug 1976
c. Total usable data points(coverage)	4591 (Newfoundland-Cuba)	2929 (Puerto Rico-N.Carolina)
d. Range of equator crossing angles	99.64°E-102.46°E	53.54°W-56.36°W
e. Strip width equator 30° latitude	 284km 265km	 284km 265km
f. Mean offset from geoid*	9.85m(SD$^+$=4.23m)	-5.54m(SD$^+$=3.74m)
g. Mean slope with respect to geoid	-4.51m/1000km (SD$^+$=1.77m/1000km)	1.00m/1000km (SD$^+$=1.39km/1000km)
h. Equator crossing of reference path	100.8700°E	55.0100°W
i. Origin for linear distance along the reference path	55.2809°W 49.2387°N (Newfoundland)	62.1475°W 12.8496°N (N. of Trinidad)

* Marsh-Vincent Goddard Space Flight Center Geoid
\+ Standard deviation

Result of GEOS-3 Data Analysis

The present analysis technique has a few arbitrary yet important variables which may produce different solutions for a given set of data. These variables include (1) number of tidal constituents sought (in addition to a geoid), (2) order of polynomial function representing a geoid as well as tides, and (3) spatial length of data. While the first two variables are attributed to the usual convergence problem resulting from incompleteness of both representation function and data, the third variable is due to the removal of the orbital drift error as described in Step 4 in the previous section.

Since these variables may significantly affect the convergence of the solution, we allowed them to vary within limited ranges. Specifically, analyses were performed for the following range of each variable:

1. Number of tidal constituents - 2 groups

   1st Group: Geoid, M_2 and O_1 tides

   2nd Group: Geoid, M_2 O_1, S_2, and K_1 tides

2. Order of polynomial - 4 groups

   5th, 6th, 7th, and 8th order Chevychev polynomials for both geoid and tides

3. Spatial length of data

   a) 4 groups for the south-going paths: 300 Km - 1,600 Km; 300 Km - 2,400 Km; 2,200 Km - 3,600 Km; and 300 Km - 3600 Km

   b) 1 group for the north-going paths; 1,000 Km - 2,900 Km

In total, 32 different analyses were performed for the south-going paths, and 8 for the north-going paths. An origin time for the entire data was arbitrarily chosen to be 00:00:00 GMT on January 1, 1975 so that all tidal phases are referenced to this time.

Incorporation of the orbital drift error into the normal equation (5) was tested for both north- and south-going data sets. When the orbital drift for each path is expressed by a linear equation in distance, the process generates additional $2N_p$ unknowns where N_p is the total number of paths used for analysis. The data preparation for this test, of course, did not include Step 4 described in the previous section. Test results showed that the coefficients of the linear equation for orbital drift thus obtained were almost identical to those obtained from Step 4. However, the increased number of normal equations caused numerical instability for high-order (7th and 8th order) polynomial representations of the geoid and tides due to the limited amount of input data. Therefore, this process was not pursued any further.

It is impractical to present all 40 different sets of solutions in this report; we present only a set of four different solutions for each strip in figures 5 and 6. Other solutions show similar tidal characteristics without significant differences. A statistical summary for all 40 solutions is shown in Table 2.

For a given spatial length of data it was found that the geoid solutions agree within 30 cm or less for all orders of polynomial and more or less independent of the number of tidal constituents. Change in the spatial data length caused only "tilting" of the geoid, mainly because the length affects the linear fitting (Step 4) during the data preparation in removing the orbital drift errors.

The residual geoids obtained from the analysis for both south- and north-going paths are plotted on the fourth graph of Figures 3 and 4. Each solution is compared with the simple arithmetic mean of the residual altimeter data. In both cases, the agreement appears to be reasonable.

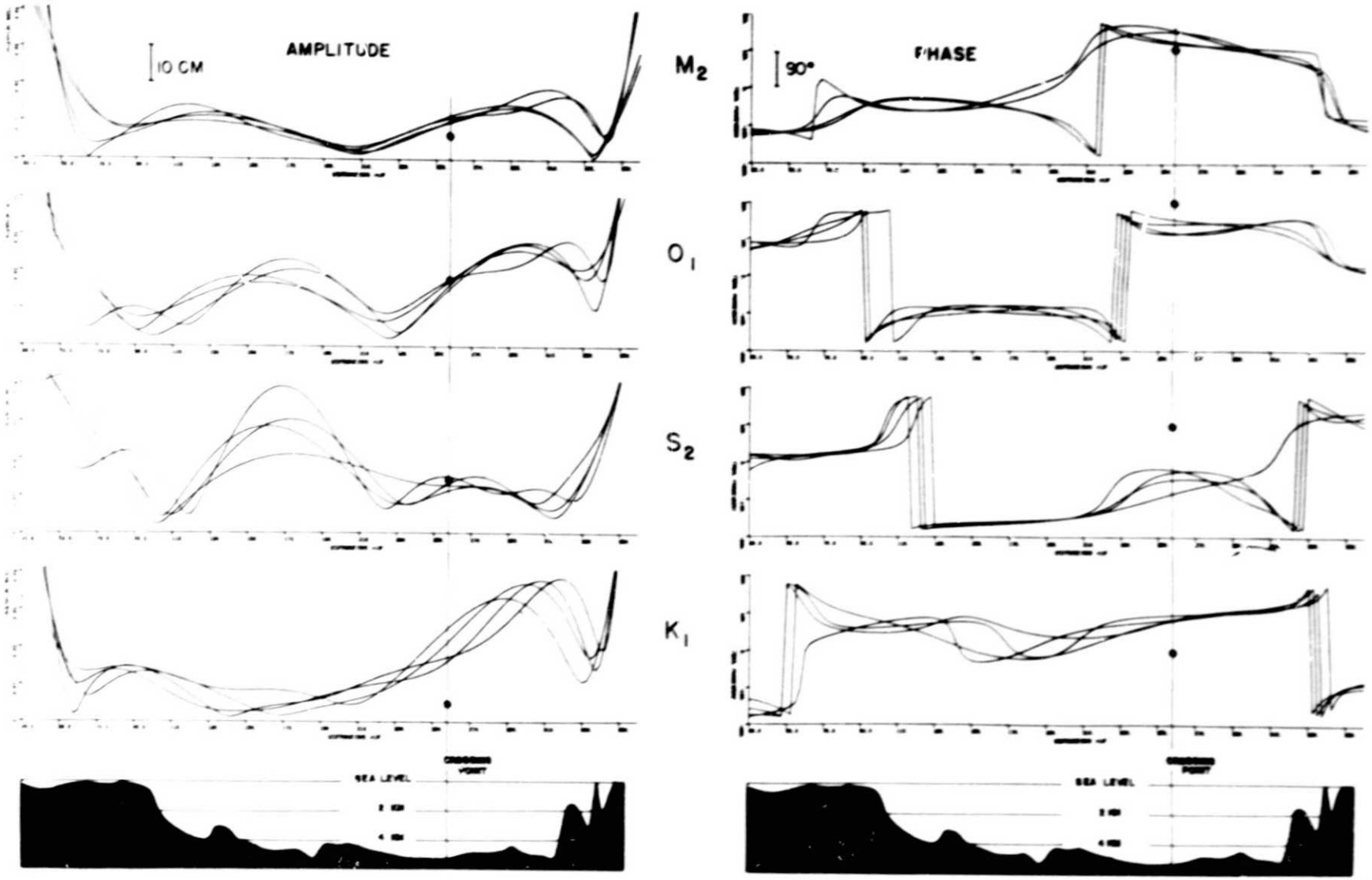

Figure 5. South-going amplitude and phase profiles for M_2, O_1, S_2 and K_1 tides obtained from altimeter data using 5th, 6th, 7th, and 8th order Tchevichev polynomial representations. As the order increases, the profile generally has more ups and downs. The residual geoids agree within 20 cm for all cases and their mean is shown in the fourth graph of Figure 3. Crossing point results compared with Figure 6 are shown in solid circles. Note that the sharp changes in phase are merely 360° shifts for plotting purposes only.

ORIGINAL PAGE IS OF POOR QUALITY

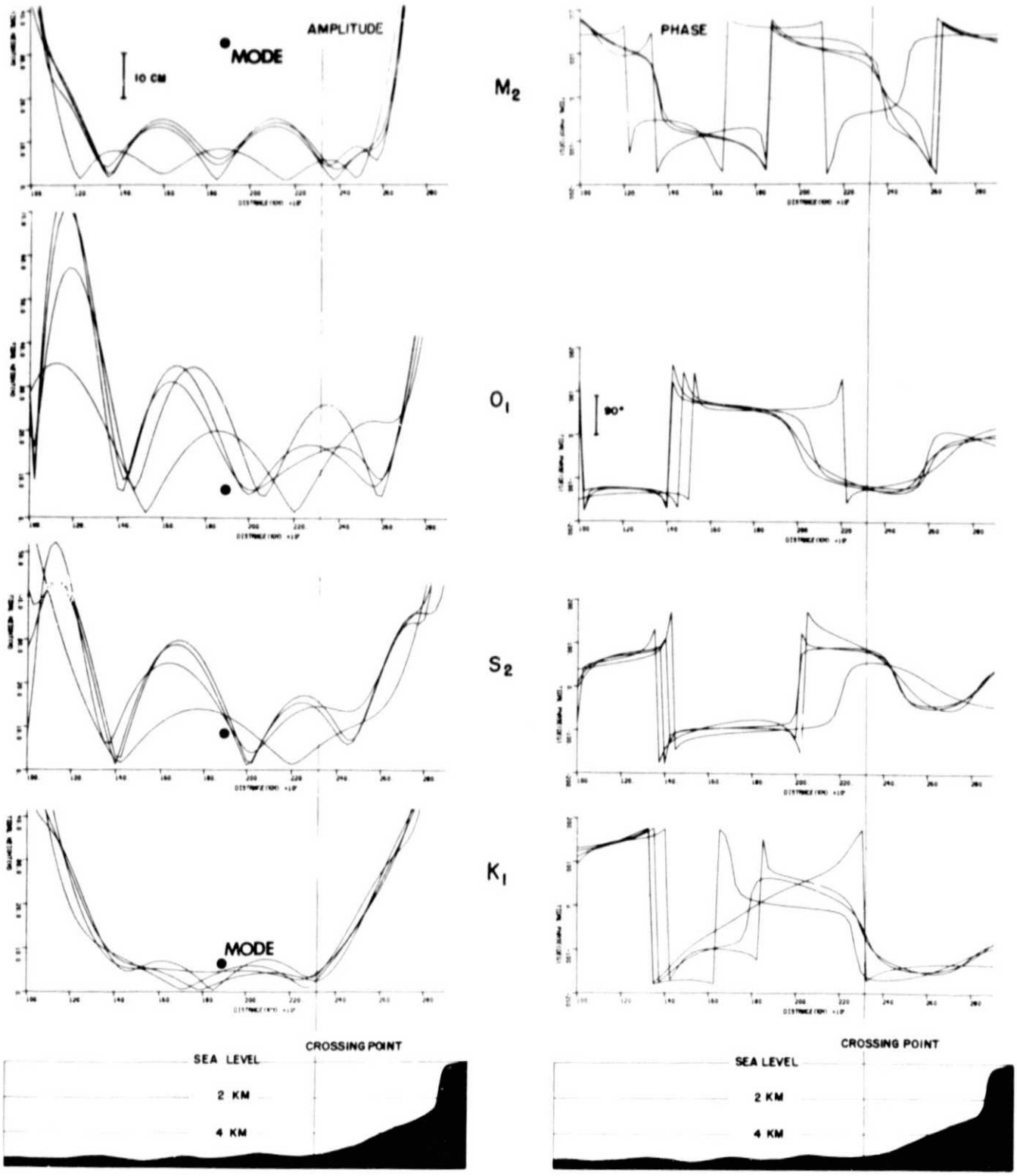

Figure 6. North-going amplitude and phase profiles for M_2, O_1, S_2, and K_1 tides. Data from MODE gauge(Figure 1) are shown in solid circles. For additional explanation refer to Figure 5.

ORIGINAL PAGE IS
OF POOR QUALITY

TABLE 2. RMS Error Amplitudes(cm) of the Residual Altimeter Data after Removing Geoid and Tides for 40 Different Analyses

Data Range (km)	total data point	(3) data RMS amplitude (cm)	RMS Error Amplitudes (cm)							
			(1) Geoid, M_2, O_1				Geoid, M_2, O_1, S_2, K_1			
			(2) 5	6	7	8	5	6	7	8
300-1600*	1671	84	60 (0.98)	53 (1.23)	50 (1.35)	47 (1.48)	58 (1.05)	50 (1.35)	46 (1.53)	42 (1.73)
300-2400*	2946	80	74 (0.41)	64 (0.75)	59 (0.92)	56 (1.06)	73 (0.45)	64 (0.75)	58 (0.95)	53 (1.13)
300-3600*	4591	151	100 (1.13)	100 (1.13)	99 (1.15)	99 (1.15)	98 (1.17)	98 (1.17)	97 (1.19)	97 (1.19)
2200-3600*	1921	101	88 (0.56)	81 (0.74)	78 (0.82)	76 (0.88)	87 (0.59)	78 (0.82)	75 (0.90)	72 (0.98)
1000-2900*	2430	214	96 (1.99)	88 (2.22)	84 (2.34)	84 (2.34)	94 (2.05)	85 (2.31)	82 (2.41)	81 (2.45)

* South-going data(28paths)
\+ North-going data(26paths)
(1)Geoid and tidal species used for analyses
(2)Order of Tchevichev polynomial to represent both geoid and tides
(3)RMS amplitude of the data after removing the orbital drift (mean=0)

Note: Bracketed figures represent the signal-to-noise ratio as defined by

$$\sqrt{\frac{(\text{RMS ampl. of data})^2 - (\text{error ampl.})^2}{(\text{error ampl.})^2}}$$

When the residual geoid thus obtained is added to the original Marsh-Vincent geoid, we obtain an "improved" geoid containing short wave length features which are not included in the original geoid model. The "improved" geoids are shown on the fifth graph of figures 3 and 4, and compared with the Marsh-Vincent ones. It is interesting to note somewhat better correlation of the "improved" geoid with bathymetric profiles. For the north-going paths, the geoidal correction amounts to as much as 6 m near the Puerto Rican Trench. However, this large deviation may be partially due to a relatively short spatial data length along these paths.

We note from Figures 5 and 6 that the four solutions for tidal amplitudes agree within about 10 cm in most cases except near margins due to familiar edge effect. Agreement on phases is somewhat poor although consistent trends are noticeable in all cases.

Figure 6 also shows the tidal amplitudes obtained from the MODE deep-sea gauge (Zetler et al, 1975). While all tidal amplitudes are within an order of magnitude not exceeding 40 cm, the agreement with the MODE data is rather poor particularly for M_2 tide. It is disturbing to note that S_2 amplitude is bigger than that of M_2 in figures 5 and 6. Considering the tidal inducing force, we expect M_2 to have greater amplitude than S_2 unless there exists an unusual spectral feedback between the two constituents in the data area. It is more likely due to the insufficient quantity and accuracy of altimeter data.

On the other hand, any ground truth data from deep sea measurement can be incorporated in the normal equations using the Lagrangian multiplier technique (Won et al, 1977). This technique was not applied in this analysis mainly because the present purpose is to compare the two different solutions.

It is anticipated that as more data are accumulated from GEOS-3 and future SEASAT series satellites with improved tracking technique, the discrepancy will resolve eventually. The main emphasis here must be that the analytic method presented here does produce a consistently converging solution, within expectation, in spite of limited quantity and quality of the altimeter data.

Conclusions

1. Mapping the ocean tides and geoid using satellite altimeter data is indeed possible in a large regional scale provided that a sufficient amount of data and reasonable altimeter accuracy are attainable.

From the viewpoint of economy and available data density, the satellite altimeter provides the most abundant and direct measurements. The satellite altimeter data can best be utilized in obtaining a geopotential model when the data are reduced simultaneously for a geoid and for a set of tidal surfaces. Large residual errors which are present in available gravity models are mainly attributed to: 1) exclusion of the tidal perturbation and, 2) ineffectiveness of the spherical harmonic expansion technique in describing localized gravity anomalies. These two factors, in addition to the measurement errors, essentially dictate the upper limit of the residuals of a gravity model, which may be on the order of a few meters or less. Some of the recent gravity models are already approaching this limit.

Considering the large number of tidal constituents, the regional treatment of the altimeter data appears to be the best approach in deriving both the static and the dynamic geopotential models. The entire ocean area may be divided into about a dozen partially overlapping regions. For each region, geoid and tide models will be derived from the altimeter data by specifying a functional surface for each model whose resolution can be much higher than those attainable by the spherical harmonic technique.

2. The oceanic geoid can be improved significantly through tidal analysis. In a strict sense, the ocean geoid obtained from the altimeter data is a time-invariant ocean surface topography with respect to the spheroid. Therefore the ocean geoid thus derived, even after tidal corrections, may still be contaminated by localized elevations created by steady-state geostrophic current systems. If the current system meanders fast enough as compared with the duration of the altimeter data, we may hope that its long-term effect on the geoid would not be significant. In addition, since the geostrophic currents occupy only a small portion of the ocean, the overall residual amplitude of a geoid can be reduced to significantly less than one meter when tides are fully accounted for.

3. Once the altimeter data are corrected for the geoid and tides, the residual altimeter data can be used to investigate transient sea surface variations which may be associated with winds and storms. The residual data may also be used to identify extremely localized geoidal features caused by small sea mounts and narrow trenches.

Acknowledgements

We are greatly indebted to H. Ray Stanley, GEOS-3 Project Manager at NASA Wallops Flight Center, for distributing the data used for this analysis. This work was funded by NASA contract NAS6-2810 through Applied Science Associates, Apex, North Carolina.

References

Brown, R. D., T. G. Masters and W. D. Kahn, GEOS-3 altimeter data noise analysis, presented at the Fall Am. Geophys. Union Meeting, San Francisco, Dec. 6-10, 1976.

Gaposchkin, E. M. and G. Mendes, Gecpotential model to degree and order 30 from satellite and terrestrial data, abstract, transactions, Amer. Geophy. Union, v. 58, 6, 371, 1977.

Kuo, J. T. and F. C. Jackson, Mapping tides in the northeastern Pacific using GEOS-3 altimeter data, Presented at the GEOS-3 Investigation Final Meeting in New Orleans, Nov. 18-19, 1977.

Lerch, F. J., J. E. Brown, and S. M. Klosko, Gravity model improvement using GEOS-3 (GEM 9 and 10), abstract, Transactions, Amer. Geophy. Union, v. 58, 6, 371, 1977.

Marsh, J. G., B. C. Douglas, S. Vincent, and D. M. Walls, Tests and comparisons of satellite derived geoids with skylab altimeter data, J. Geophy. Res., v. 81, 20, 3594-3598, 1974.

Maul, G. A., and A. Yanaway, Deep Sea tide determination from GEOS-3, Report to NASA Wallops Flight Center, October 1977.

National aeronautics and Space Administration, SEASAT-A Program Summary, 1975.

Rapp, R. H., The Geoid: definition and determination, Transaction, Amer. Geophy. Union, 55, 118-126, 1974.

Stanley, H. R. and L. S. Miller, Analysis of GEOS-3 data for ocean and land areas, abstract, Transaction, Amer. Geophy. Union, v. 58, 6, 369, 1977.

Tiron, K. D., Y. N. Sergeev, and A. N. Michurin, Maps of tides in the Pacific, Atlantic, and Indian Oceans, Vest. Leningrad Union, 24, 123-135, 1967.

Won, I. J., J. T. Kuo and R. C. Jachens, Mapping ocean tides with satellite - a computer simulation, abstract, Trans. Amer. Geophy. Union, v. 58, 6, 370, 1977.

Zettler, B. D. and G. A. Maul, Precision requirements for a spacecraft tide program, J. Geophys. Res., 76, 27, 6601-6605, 1971.

_____, W. Munk, H. Mofjeld, W. Brown, and F. Dormer, MODE tides, J. Phys. Oceano., 5, 430-441, 1975.